Coherent population trapping magnetometer by differential detecting magneto–optic rotation effect*

Fan Zhang(张樊), Yuan Tian(田原), Yi Zhang(张奕), and Si-Hong Gu(顾思洪)†

Key Laboratory of Atomic Frequency Standards, Wuhan Institute of Physics and Mathematics, Chinese Academy of Sciences, Wuhan 430071, *China*

(Received 9 March 2016; revised manuscript received 13 April 2016; published online 2 August 2016)

A pocket coherent population trapping (CPT) atomic magnetometer scheme that uses a vertical cavity surface emitting laser as a light source is proposed and experimentally investigated. Using the differential detecting magneto–optic rotation effect, a CPT spectrum with the background canceled and a high signal-to-noise ratio is obtained. The experimental results reveal that the sensitivity of the proposed scheme can be improved by half an order, and the ability to detect weak magnetic fields is extended one-fold. Therefore, the proposed scheme is suited to realize a pocket-size CPT magnetometer.

Keywords: coherent population trapping, atomic magnetometer, magneto–optic rotation effect

PACS: 42.50.Gy, 07.55.Ge, 33.57.+c, 78.20.Ls **DOI:** 10.1088/1674-1056/25/9/094206

1. Introduction

Magnetometers play an important role in detecting the Earth's magnetic field, space physics, and biomedical and other fields.[1–4] With the development of laser spectroscopy and quantum optics, highly sensitive magnetometers based on light–atom interactions have been extensively studied.[5–7] Magnetometers with coherent population trapping (CPT) use an all-optical system,[8–11] and because of their small size, low power consumption, and low cost, they are competitive.

Small size CPT magnetometers generally use circularly polarized light that is converted from linearly polarized light emitted by a vertical cavity surface emitting laser (VCSEL). A direct current modulated at a microwave frequency of 3.417 GHz drives the VCSEL to emit a multi-chromatic light beam, and then the multi-chromatic light beam propagates into the alkali atom cell. The ± 1 sidebands of the multi-chromatic light interact with the alkali atoms, leading to CPT. The magnitude of magnetic flux density B can be determined by detecting the transmission light and analyzing the CPT signal (defined as the prevalent scheme). The achieved miniature CPT magnetometer is exactly based on the prevalent scheme.[8] However, the CPT signal quality of the prevalent scheme is not optimal, so its sensitivity is reduced.

The main factors affecting the quality of the CPT signal include the following: 1) only the ± 1 sidebands of the multi-chromatic light carry the CPT information, and other unwanted sidebands only contribute amplitude noise (AM noise), which means that the background is much larger than the CPT signal;[12] 2) the laser outputted by a VCSEL has a wide spectral bandwidth of approximately 100 MHz, and the frequency noise from frequency jitter is converted into amplitude noise (FM–AM noise). Therefore, the CPT signal has strong FM–AM noise;[13] and 3) circularly polarized light pumps the atoms to the spin-polarized dark state, so the number of interacting atoms will be reduced.[14]

Linearly polarized light can overcome the problem of the spin-polarized dark state and produce a better-quality CPT signal.[15] Employing a better laser source can also improve the quality of the CPT signal. Feng's group used narrow bandwidth linearly polarized light[16] and Lin's group also obtained narrow bandwidth linearly polarized dichromatic light using an optical phase-lock loop.[17] They both have observed high-quality CPT signals. However, these two laser sources have a large size and are expensive, making it difficult to realize practical magnetometers.

The magneto–optic rotation effect in CPT has been studied in Ref. [18], and we have studied a differential magneto–optic rotation (DMOR) atomic clock scheme that uses linearly polarized multi-chromatic light to interact with ^{87}Rb atoms.[19] Based on this scheme, we also experimentally study the DMOR CPT magnetometer scheme. The research results are given below.

In our experiment, ^{87}Rb is employed as the interacting atom. The linear polarized dichromatic light propagating along the direction of the magnetic field B can be divided into left and right circularly polarized components, which interact with ^{87}Rb as shown in Fig. 1(a). Under a weak B, the ground state hyperfine energy sublevels linearly shift with B field and hyperfine level splits are expressed by Breit–Rabi formula $\hbar\omega_{m_1,m_2} \approx \hbar\omega_{0,0} + (m_1 + m_2)\gamma B$, where m_1 and m_2 are respectively the azimuthal quantum numbers for the $F_g = 1$ and $F_g = 2$ states, ω_{m_1,m_2} is the microwave angular frequency between two involved sublevels, and γ is the gyromagnetic

*Project supported by the National Natural Science Foundation of China (Grant Nos. 11304362 and 61434005).

†Corresponding author. E-mail: shgu@wipm.ac.cn

© 2016 Chinese Physical Society and IOP Publishing Ltd

ratio of the atom. When dichromatic light, with optical angular frequency ω_1, and ω_2, is Raman resonant with atoms through a Λ configuration, that is $\hbar\omega_1 - \hbar\omega_2 = \hbar\omega_{m_1,m_2} \approx \hbar\omega_{0,0} + (m_1 + m_2)\gamma B$, the CPT spectral line can be observed and thus the B field intensity can be decided.

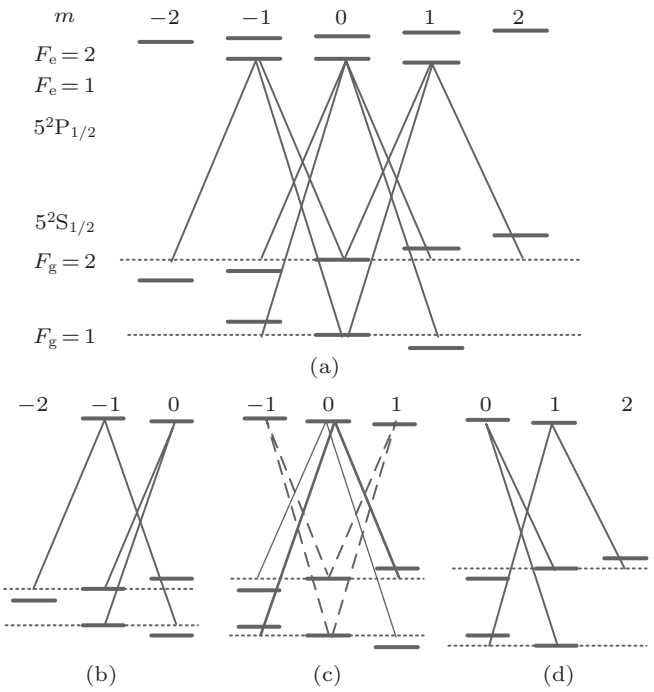


Fig. 1. (a) Transition scheme for the linearly polarized dichromatic light interacting with ^{87}Rb atoms. Panels (b), (c), and (d) respectively represent the Raman resonance of the Λ configurations with two hyperfine ground states satisfying $m_1 + m_2 = -2$, $m_1 + m_2 = 0$, and $m_1 + m_2 = 2$.

From Fig. 1(a), it is seen that the dichromatic field can generate several Λ configuration CPT resonances. When the dichromatic field is Raman resonant with two $m_{1,2} = -1$ sub-states, as shown in Fig. 1(b), it is resonant with $m_1 = 0$ and $m_2 = -2$ sub-states as well. Therefore, two Λ configuration CPT resonances with $m_1 + m_2 = -2$ will happen simultaneously. When the field is Raman resonant with two $m_{1,2} = 0$ sub-states, there exist four Λ configuration CPT resonances corresponding to $m_1 + m_2 = 0$ as shown in Fig. 1(c). However, as the CPT resonances of the two Λ configurations marked with broken lines are destructive interference, only the CPT resonances from the other two can be observed. Similar to Fig. 1(b), when the dichromatic field is Raman resonant with two $m_{1,2} = 1$ sub-states as shown in Fig. 1(d), there appear two Λ configuration CPT resonances with $m_1 + m_2 = 2$.

2. Experimental setup

Our experimental setup is shown in Fig. 2. A DC modulated at a microwave frequency of 3.417 GHz drives a VCSEL to emit linearly polarized multi-chromatic light. The proper DC allows the sideband of the multi-chromatic light to fit the D1 line of ^{87}Rb, and the proper microwave modulation index allows the ± 1 sidebands' power to become as strong as possible. The attenuator is used to adjust the laser intensity, and the $\lambda/2$ plate is used to rotate the polarization direction of the linearly polarized light. The ^{87}Rb cylindrical cell is 40 mm long and 25 mm in diameter, containing 4-Torr N_2–CH_4 (the ratio of N_2 to CH_4 is 1:2) as a buffer gas. A solenoid is coiled outside of the cell to provide B parallel to the laser beam. The cell and the solenoid are placed in a 3-layer permalloy magnetic shield to eliminate any environmental stray electro–magnetic field. The PBS separates the laser beam that has interacted with atoms into two beams that are mutually perpendicular. Two of the identical PDs separately detect the transmission beam and reflected beam of the PBS. The $\lambda/4$ plate can be moved in or out of the light path before the cell as required.

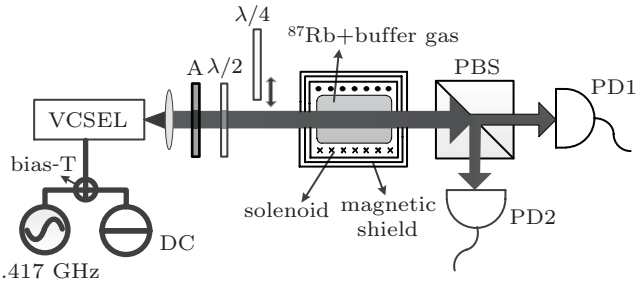


Fig. 2. Experimental setup. DC: direct current. A: attenuator. $\lambda/2$: half-wave plate. $\lambda/4$: quarter-wave plate. PBS: polarization beam splitter. PD1, PD2: photoelectric detectors.

The temperature of the cell and the VCSEL are separately controlled in the experiment. To stabilize the laser frequency at the $F_e = 1$ excited state, the temperature of the cell cannot be too high, to ensure this $F_e = 1$ spectrum line can be clearly resolved.[20] The cell is stabilized at 45 °C, and the VCSEL is stabilized at 25 °C.

3. Results and discussion

Under the condition that the multi-chromatic light does not exhibit Raman resonance with ^{87}Rb, rotating the $\lambda/2$ plate and adjusting the polarization direction of linearly polarized light can cause the intensity of the two output beams of the PBS to be equal. Therefore, the differential signal of the two PDs' output is almost 0. When the ± 1 sidebands exhibit Raman resonance with atoms, the polarization direction of the ± 1 sidebands will rotate because of the magneto–optic rotation effect. Therefore, their contributions to the two PDs are not equal anymore and the CPT signal will be detected. However, the polarization of other unwanted sidebands will not rotate and their contributions to the two PDs will be canceled. Therefore, the CPT signal in the differential signal of the two PDs is totally attributed to the ± 1 sidebands.

The DMOR scheme CPT signal shown in Fig. 3(a) is the differential signal of the two PDs' output. To compare the DMOR scheme with the prevalent scheme, a $\lambda/4$ plate

is placed before the cell to convert linearly polarized light to right circularly polarized light, and the prevalent scheme CPT signal shown in Fig. 3(a) is the sum signal of the two PDs' output. Because the right circularly polarized light pumps a certain amount of atoms to the $m = 2$ spin-polarized dark state which reduces the CPT signal amplitude, and the pumping also causes the $m_1 + m_2 = 2$ CPT signal amplitude to be larger than that of $m_1 + m_2 = -2$ in Fig. 3(a). The quality of the CPT signal is also affected by the strong background signal. From the Fig. 3(a) prevalent scheme curve, it is seen that the ratio of the $m_1 + m_2 = 2$ CPT signal to its background is approximately 3%. However, the differential detecting makes the background of the DMOR CPT signal be nearly 0. In Fig. 3(a), it is seen that due to the different rotation direction between $m_1 + m_2 = -2$ and $m_1 + m_2 = 2$ CPT resonances, the $m_1 + m_2 = -2$ DMOR CPT signal and $m_1 + m_2 = 2$ DMOR CPT signal have opposite signs. Another characteristic of the DMOR curve is that the $m_1 + m_2 = 0$ CPT signal is approximately one order weaker than that of $m_1 + m_2 = \pm 2$, and its amplitude and linewidth are sensitive to B.[19] We also frequency modulate the microwave at 1 kHz and obtain the differential style lock-in CPT signal using a lock-in amplifier. Figure 3(b) shows the differential type lock-in CPT signal. According to Fig. 3, the DMOR scheme CPT signal amplitude is larger than that of the prevalent scheme by about 1.8 times because the linearly polarized light can overcome the problem of the spin-polarized dark state, and the DMOR scheme has a better signal-to-noise ratio.

Because the performance of the VCSEL is poor, the noises from the VCSEL's light intensity instability and frequency jitter are strong, especially for FM–AM noise. Fortunately, these noises are all common mode noises, so they can be suppressed by differential detection. Therefore, the noise amplitude of the DMOR scheme is lower than that of the prevalent scheme, as shown in Fig. 4, the microwave frequency was fixed at a zero Raman detuning of $m_1 + m_2 = 2$, and B was stepped in 6 s intervals with a step length of 4.8 nT. According to Fig. 4, the prevalent scheme nearly reaches its limit of resolution. However, the DMOR scheme can measure smaller variations of B. To compare the noise of these two schemes, figure 5 shows the power spectrum density of the two schemes in units of magnetic flux density with a fixed microwave frequency at a zero Raman detuning of $m_1 + m_2 = 2$. Figure 5 reveals that the DMOR scheme curve presents less noise in the whole bandwidth range, and its sensitivity is half an order better than that of the prevalent scheme.

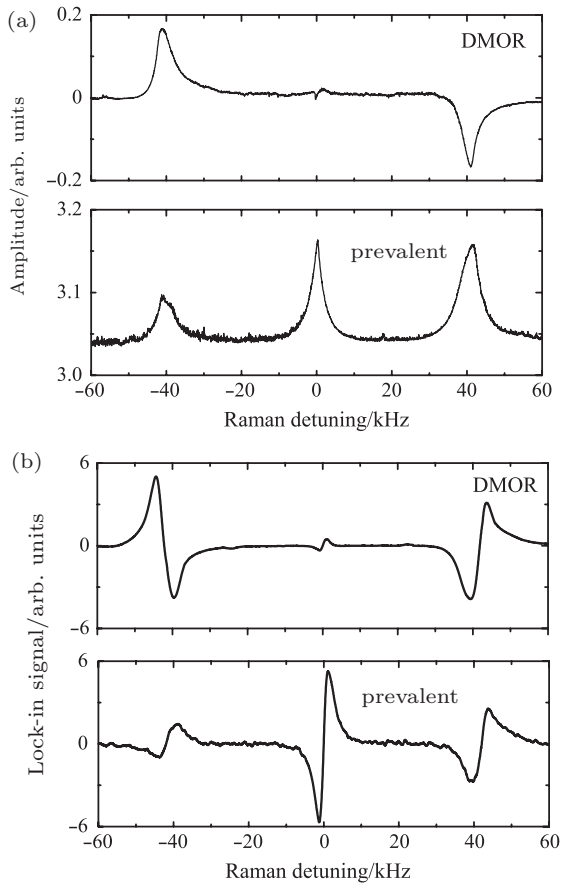


Fig. 3. The modulation frequency is 1 kHz, the lock-in time constant is 50 ms, the voltage sensitivity of the lock-in amplifier is 5 mV, the laser intensity is 3 mW/cm^2, and $B = 3$ μT. (a) CPT signal, (b) lock-in CPT signal.

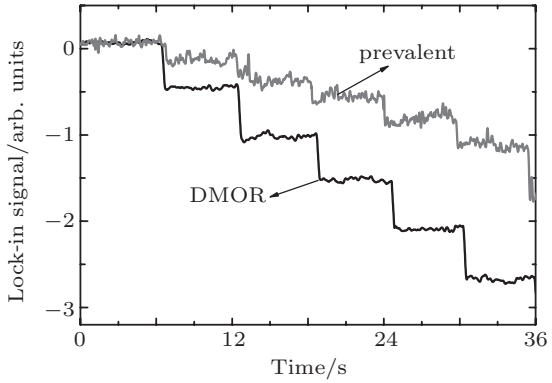


Fig. 4. The lock-in signal is plotted as a function of time when B is stepped in 6 s intervals with a step length of 4.8 nT, the other parameters are the same as those of Fig. 3.

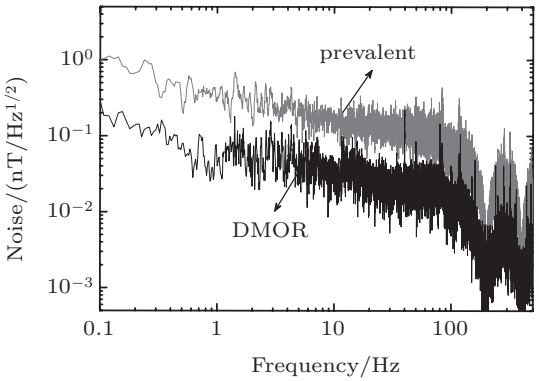


Fig. 5. Power spectral density of the lock-in signal. The lock-in time constant is 640 μs, with a filter roll-off of 24 dB/octave, the other parameters are the same as those of Fig. 3.

The magnetic field can be determined by analyzing the microwave frequency difference between the nearest CPT signals. Because the $m_1 + m_2 = 0$ CPT signal of the DMOR scheme can be ignored when B is weak, the DMOR scheme can extend the ability to detect a weak B one-fold relative to the prevalent scheme. Our group has proposed an energy level modulation (ELM) scheme,[9] which obtained a similar CPT signal to the DMOR scheme. Although the ELM scheme has the same ability to detect a weak B as the DMOR scheme, it cannot cancel the background and suppress the noise, and it requires another solenoid, which increases the volume and complexity of the system. Therefore, the DMOR scheme has more advantages.

The CPT magnetometer that uses a VCSEL as the laser source has the advantages of small size and high spatial resolution. Compared with the prevalent scheme, the DMOR scheme only adds a PBS and a photoelectric detector. Its spatial resolution remains unchanged and its detector volume slightly increases. Furthermore, the circuit resource for the DMOR scheme remains at the same level as the prevalent scheme.

4. Conclusion

We experimentally investigated a CPT magnetometer scheme based on differential magneto–optic rotation (DMOR) using a VCSEL as the laser source. The DMOR scheme uses linearly polarized light to overcome the problem of the spin-polarized dark state to increase the efficiency of atoms. Because of the differential detection, the DMOR scheme cancels the background and suppresses common mode noise, such as FM–AM noise. According to the comparison experiment, the signal-to-noise ratio is improved and the sensitivity of the DMOR scheme is half an order better than that of the prevalent scheme. In addition, the DMOR scheme extends the ability to detect a weak B one-fold. However, the spatial resolution, the size, the power consumption, and other resources of the DMOR magnetometer scheme are almost the same as that of the prevalent scheme. Therefore, the DMOR CPT magnetometer scheme is an ideal scheme to realize miniature magnetometers.

References

[1] Kirschvink J L, Maine A T and Vali H 1997 *Science* **275** 1629
[2] Harry G M, Jin I, Paik H J, Stevenson T R and Wellstood F C 2000 *Appl. Phys. Lett.* **76** 1446
[3] Baule G and Mcfee R 1963 *Am. Heart J.* **66** 95
[4] Hamalainen M, Hari R, Ilmoniemi R J, Knuutila J and Lounasmaa O V 1993 *Rev. Mod. Phys.* **65** 413
[5] Affolderbach C, Stahler M, Knappe S and Wynands R 2002 *Appl. Phys. B* **75** 605
[6] Cartaleva S, Karaulanov T, Petrov N, Slavov D, Vaseva K, Yanev A, Mijailovic M, Grujic Z and Jelenkovic B 2007 *Acta Phys. Pol. A* **112** 871
[7] Pustelny S, Wojciechowski A, Kotyrba M, Sycz K, Zachorowski J, Gawlik W, Cingoz A, Leefer N, Higbie J M, Corsini E, Ledbetter M P, Rochester S M, Sushkov A O and Budker D 2007 14*th International School on Quantum Electronics: Laser Physics and Applications*, September 18–22, 2006, Sunny Beach, Bulgaria, p. 60404
[8] Schwindt P D D, Knappe S, Shah V, Hollberg L, Kitching J, Liew L A and Moreland J 2004 *Appl. Phys. Lett.* **85** 6409
[9] Liu G B and Gu S H 2010 *J. Phys. B-At. Mol. Opt. Phys.* **43** 035004
[10] Liang S Q, Yang G Q, Xu Y F, Lin Q, Liu Z H and Chen Z X 2014 *Opt. Express* **22** 6837
[11] Belfi J, Bevilacqua G, Biancalana V, Dancheva Y and Moi L 2007 *J. Opt. Soc. Am. B-Opt. Phys.* **24** 1482
[12] Vanier J, Levine M W, Janssen D and Delaney M 2003 *Phys. Rev. A* **67** 065801
[13] Camparo J C and Coffer J G 1999 *Phys. Rev. A* **59** 728
[14] Zhang Y, Qu S P and Gu S H 2012 *Opt. Express* **20** 6400
[15] Zibrov S A 2010 *Phys. Rev. A* **81** 013833
[16] Hu Y, Feng Y Y, Xu C, Xue H B and Sun L 2014 *Appl. Optics* **53** 2158
[17] Yang A L, Yang G Q, Xu Y F and Lin Q 2014 *Chin. Phys. B* **23** 027601
[18] Pradhan S, Kani A, Wanare H, Behera R and Das A K 2012 *Phys. Rev. A* **85** 063805
[19] Tan B Z, Tian Y, Lin H F, Chen J F and Gu S H 2015 *Opt. Lett.* **40** 3703
[20] Taichenachev A V, Yudin V I, Velichansky V L and Zibrov S A 2005 *Jetp. Lett.* **82** 398